LHCb Collaboration

LHCB 99-034 CALO
September 7, 1999

Optimization of cell sizes of electromagnetic calorimeter

S.Barsuk[1], **I.Belyaev**[2], **A.Golutvin**[3], **I.Korolko**[4]
ITEP, Moscow, Russia

[1] Sergey.Barsuk@itep.ru
[2] Ivan.Belyaev@itep.ru
[3] Andrey.Golutvin@cern.ch
[4] Ivan.Korolko@cern.ch

Contents

1 Introduction to the calorimeter options

The electromagnetic calorimeter, described in the Technical Proposal (TP) [1], consists of three sections with different cell sizes: 4×4, 8×8, and 16×16 cm^2. The TP design was mainly optimized to provide high efficiency electron trigger. This note describes re-optimization studies aimed to:

- simplify the design of the calorimeter, in particular minimize the number of sections with various transversal granularity;
- maximize the efficiency for π^0 reconstruction.

The trigger efficiency and total number of channels were supposed to be kept at the same level as the TP design. Two options of the calorimeter (each consisting of two sections) have been studied and compared with the TP design in terms of efficiency for π^0 -reconstruction. The parameters of the TP and newly studied options, referred as 4×12 and 6×12, are listed in table 1. In contrast to so-far-never-constructed 16×16 cm^2 module, the module in the outer section of 4×12 and 6×12 options has the lateral size of 12×12 cm^2. The modules of this size have been successfully constructed and tested for the HERA-B electromagnetic calorimeter.

Table 1: Calorimeter options description

TP-rec Calorimeter Description			
# of zone	Cell size	Zone outer size (in 32x32cm blocks)	# of channels
1	4cm	8x6	2816
2	8cm	14x10	1472
3	16cm	26x20	1520
Total			5808
4-12 Calorimeter Description			
# of zone	Cell size	Zone outer size (in 24x24cm blocks)	# of channels
1	4cm	10x8	2624
2	12cm	34x26	3216
Total			5840
6-12 Calorimeter Description			
# of zone	Cell size	Zone outer size (in 24x24cm blocks)	# of channels
1	6cm	10x8	1120
2	12cm	34x26	3216
Total			4396

The dimensions of inner modules are 4×4 and 6×6 cm^2 for the 4×12 and 6×12 options correspondingly. The latter option has significantly smaller number of channels as compared with the TP design. The geometry of calorimeter cell size arrangement is shown in Figure 1 for TP-rec version and for proposed two-zone 4-12 version.

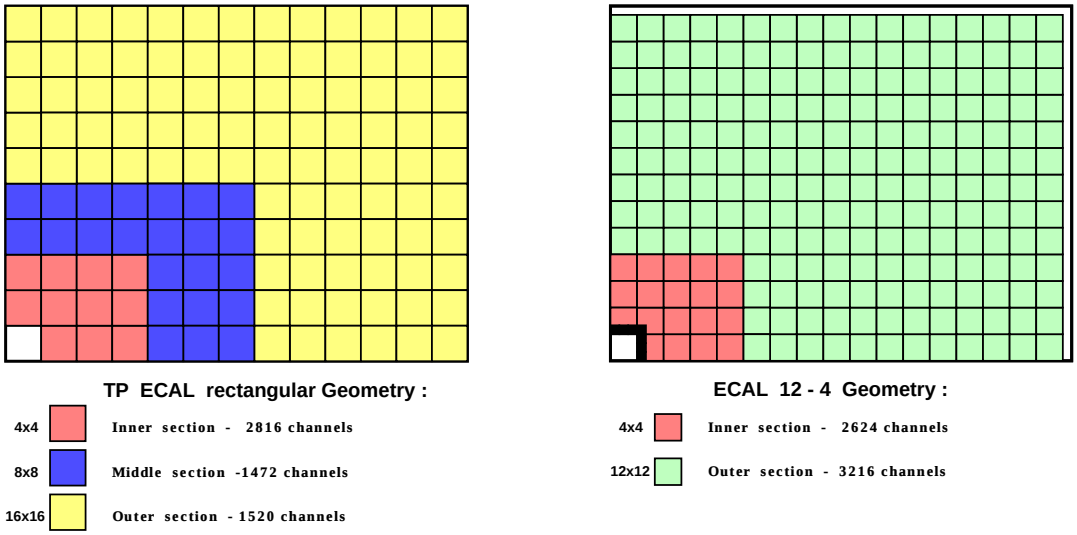

Figure 1: One quarter of the LHCb electromagnetic calorimeter shown for two options: left - simplified "rectangular" geometry which is close to the calorimeter described in the TP (dimension of one block is 32x32 cm^2), right - proposed two-zone calorimeter with cells of 4×4 and 12×12 cm^2 (dimension of one block is 24x24 cm^2)

2 Test reactions

As shown in [2] all three options considered have nearly identical trigger efficiency. To study π^0 reconstruction we used a set of key reactions. Below B $\to \rho\pi$, B $\to$ DK*, b $\to \gamma$X decays are discussed. π^0s from B decays can be produced in the wide momentum interval. We have therefore studied π^0 reconstruction in the two illustrative reactions: B $\to \rho\pi$ and B $\to$ DK*.

The reaction B $\to \rho\pi$, followed by $\rho \to \pi\pi$, results in the $\pi^+\pi^-\pi^0$ final state, where π^0s are produced with a relatively high momentum. Underlined problem here is that both gammas from the same π^0 often overlap and

form one cluster in the calorimeter. Physics, analysis, cuts and background suppression are described in detail in [1, 3].

The reaction $B \to DK^*$ followed by $D \to K^-\pi^+\pi^0$, results in the final state with π^0 in the intermediate momentum region, where the photons from the same π^0 have only a small probability to overlap. On the other hand due to their softer momenta the pile-up effect becomes significant. The physics and analysis procedure for $D \to K^-\pi^+$ is described in detail in [1]. According to [1] one can expect about 45 events of the type $B \to D^0K^{*0}$ to be collected and reconstructed after one year of operation. One can speculate that if the π^0 reconstruction efficiency exceeds 30% then due to a very large ratio $\frac{\mathcal{B}(D^0\to K^-\pi^+\pi^0)}{\mathcal{B}(D^0\to K^-\pi^+)} = 3.62 \pm 0.24$ [4], the number of events can be even doubled.

Another aspect of optimization is to study the separation of γs against π^0s. This is of particular importance for low multiplicity radiative penguins $b \to \gamma X$, which produce the photons in the highest possible momentum region, where discrimination between overlapped π^0s and photons is difficult. The analysis, cuts, trigger and background suppression are described in detail in [5].

3 Reconstruction of π^0

In order to reconstruct π^0 meson we applied a rather simple clusterisation procedure. Each 3×3 cells matrix with a local maximum energy deposition at its center was defined as a cluster. So defined clusters can partially overlap if there is only a single cell between two neighbour maxima. When reconstructing π^0's from photon clusters[5] three contributions to energy deposition have been taken into account:

- The energy from the genuine photon produced in the π^0 decay;
- The energy from the second photon produced in the same π^0 decay (referred further as feed-down). This case corresponds to overlapped or partially overlapped clusters. If two partially overlapped clusters are found in the calorimeter the energy in the cells common to both clusters is redistributed between clusters proportional to the energies deposited in their central cells;
- Other activity in the electromagnetic calorimeter (referred further as pile-up)

[5] only π^0s with decay photons hitting the same ECAL region were used in our analysis

The shape and the width of a π^0 signal are determined by the contribution from the above-mentioned three sources of energy deposit, which compete in a different way depending on the reaction. More details addressing $B^0 \to \rho^0\pi^0$ decay can be found in the appendix A.

The position of the cluster was determined using the "S-wave" correction procedure assuming that photons originate from the region of the interaction point. The "S-wave" correction functions were calculated for each cell size. At the boundaries between the calorimeter sections the clusters were constructed from the cells identical in size to the central cell (if possible) , i.e. few smaller cells were combined to the larger one. In future realistic clusterisation analysis has to be developed (in particular treatment of the cluster at the boundaries requires special "S-wave" correction functions). This should certainly lead to some degradation in the cluster reconstruction efficiency in the vicinity of boundaries.

The obtained information about the cluster energy and position allows to construct the 4-momentum vectors with constraint $\mathrm{E} = |\vec{\mathrm{p}}|$, referred in future as reconstructed photons.

Table 2: Summary table for $\mathrm{B}^0 \to \rho^0\pi^0$ reconstruction. The total number of Monte Carlo events which could be reconstructed ($\#^{\mathbf{MC}}_{\mathrm{B}^0}$), the number of reconstructed B^0s within $\pm 2\sigma$ ($\#^{\mathbf{REC}}_{\mathrm{B}^0}$), reconstruction efficiency (ϵ_{B^0}), the mass resolutions of π^0 (σ_{π^0}) and B^0 (σ_{B^0}) are listed.

Option	$\#^{\mathbf{MC}}_{\mathrm{B}^0}$	$\#^{\mathbf{REC}}_{\mathrm{B}^0}$	ϵ_{B^0} [%]	σ_{π^0} [MeV/c^2]	σ_{B^0} [MeV/c^2]
TP-rec-4	3362	725	21	7	63
TP-rec-8	1601	380	23	10	83
TP-rec-16	2113	420	19	11	95
TP-rec-8+16	3714	800	22		
TP-rec	7076	1525	22		
NEW-4	3258	722	22	7	64
NEW-6	3258	352	10	10	72
NEW-12-I	1774	228	12	14	117
NEW-12-II	1989	619	31	9	95
NEW-12-I+II	3763	849	23		
NEW-4+12	7021	1571	22		
NEW-6+12	7021	1201	17		

4 $B \to \rho\pi$ decay

The comparison between different geometries of ECAL is presented in tables 2 and 3 for $B^0 \to \rho^0\pi^0$ and $B^0 \to \rho^\pm\pi^\mp$ decays respectively. Used cuts on photons are identical to those applied in the analysis described in the Technical Proposal. The zone covered with 12x12 cm^2 cells is divided into NEW-12-I and NEW-12-II zones which coincide geometrically with TP-rec-8 and TP-rec-16 zones. Only reconstructed "clusters" closest to the expected impact points of the Monte Carlo photons from signal π^0 are considered, thus neglecting combinatorial background [6]. For charged tracks pure Monte Carlo information is used to reconstruct B-mesons.

As seen from tables 2 and 3 the 4-12 and TP-rec options have similar efficiency to reconstruct $B \to \rho\pi$ decay. A degradation of efficiency in the NEW-12-I zone (with respect to TP-rec-8) is fully compensated by a gain in the NEW-12-II zone (with respect to TP-rec-16). Moreover since some efficiency loss is unavoidable at the boundaries between ECAL sections with different cell size, the 4-12 option has further advantages (along with simpler construction). The 6-12 ECAL option has degraded efficiency in the inner NEW-6 section.

Table 3: Summary table for $B^0 \to \rho^\pm\pi^\mp$ reconstruction. The total number of Monte Carlo events which could be reconstructed ($\#_{B^0}^{\mathbf{MC}}$), the number of reconstructed B^0s within $\pm 2\sigma$ ($\#_{B^0}^{\mathbf{REC}}$), reconstruction efficiency (ϵ_{B^0}), the mass resolutions of π^0 (σ_{π^0}) and B^0 (σ_{B^0}) are listed.

Option	$\#_{B^0}^{\mathbf{MC}}$	$\#_{B^0}^{\mathbf{REC}}$	ϵ_{B^0} [%]	σ_{π^0} [MeV/c^2]	σ_{B^0} [MeV/c^2]
TP-rec-4	2150	538	25	7	42
TP-rec-8	966	285	29	10	59
TP-rec-16	1276	311	24	12	74
TP-rec-8+16	2242	596	26		
TP-rec	4392	1134	26		
NEW-4	2097	546	26	7	46
NEW-6	2097	291	13	11	51
NEW-12-I	1032	160	15	16	66
NEW-12-II	1187	393	33	8	65
NEW-12-I+II	2219	553	25		
NEW-4-12	4316	1099	25		
NEW-6-12	4316	844	20		

[6] Figure 10.5 in the Technical Proposal shows π^0 signal reconstructed in min.bias events taking into account combinatorial background with a signal to background ratio of about unity. We do not expect severe deterioration of the π^0 signal in B decays.

5 $B \to DK^*$ decay

Reconstruction of the decay chain $B \to DK^*$ followed by $D^0 \to K^-\pi^+\pi^0$ has been done with several intermediate mass constraints. For all charged tracks the Monte Carlo truth information has been used.

Resolution for π^0, D^0 and B^0, and the efficiency of reconstruction are shown in table 4 for TP-rec calorimeter and in table 5 for 4-12 and 6-12 calorimeter. In this reaction π^0s are much softer and therefore pile-up is relatively more important. It leads to higher tails in the mass distributions and as a consequence to a loss of reconstruction efficiency. This loss is rather significant for inner section of 6-12 solution. The situation in outer section is not so clear. 12×12 cells in the outermost region (marked as 12×12 (I) in the table) are obviously better for π^0 reconstruction than 16×16 cells. At the same time intermediate region (marked as 12×12 (II)) filled with 12×12 cells suffers from some loss of efficiency and increased widths of all mass distributions in comparison with old 8×8 scheme. This fact is however compensated by simplicity of construction of two-zone calorimeter, moreover one should also take into account unavoidable losses on the borders between zones with different cell sizes. The efficiency of B meson reconstruction in the whole outer region of 4-12 calorimeter (36.5%) is even slightly higher in comparison with that averaged over outer and middle regions of TP-rec calorimeter (35.3%).

Table 4: Results of the reconstruction of π^0,D^0 and B^0 for TP-rec option of the calorimeter. The mass resolution of π^0,D^0 and B^0 and the reconstruction efficiency for B^0 are listed

Signal	Cells [cm^2]	σ_M [MeV/c^2]	$\#^{\mathbf{MC}}_{B^0}$	$\#^{\mathbf{REC}}_{B^0}$	ε_{B^0} [%]
π^0	4×4	11			
D^0	4×4	18			
B^0	4×4	15	4649	1610	34
π^0	8×8	12			
D^0	8×8	22			
B^0	8×8	17	1956	708	36
π^0	16×16	15			
D^0	16×16	29			
B^0	16×16	25	2845	987	34

Table 5: Results of the reconstruction of π^0,D^0 and B^0 for 4-12 and 6-12 options of the calorimeter. The mass resolution of π^0,D^0 and B^0 and the reconstruction efficiency for B^0 are listed

Signal	Cells [cm^2]	σ_M [MeV/c^2]	$\#^{\mathbf{MC}}_{B^0}$	$\#^{\mathbf{REC}}_{B^0}$	ε_{B^0} [%]
π^0	4×4	12			
D^0	4×4	16			
B^0	4×4	15	4451	1538	34
π^0	6×6	21			
D^0	6×6	23			
B^0	6×6	22	4451	1266	28
π^0	12×12 (I)	22			
D^0	12×12 (I)	27			
B^0	12×12 (I)	26	2223	690	31
π^0	12×12 (II)	12			
D^0	12×12 (II)	25			
B^0	12×12 (II)	23	2641	1087	41

6 $b \to \gamma X$ decays

Good discrimination of γs against overlapped π^0s in the inner section of the LHCb calorimeter is crucial for efficient reconstruction of low-multiplicity radiative penguins, described in detail in [1, 5]. Important features of these decays are listed below:

- These decays are very sensitive to phenomena of New Physics.
- Some observable ratios allow us for almost model independent determination of the ratio of CKM elements, e.g. the ratio $\frac{\mathcal{B}(B\to\rho\gamma)}{\mathcal{B}(B\to K^*\gamma)}$ is proportional to $\left|\frac{V_{td}}{V_{ts}}\right|^2$.
- A large (up to 60-70%) SUSI-induced $\mathcal{CP}$-asymmetry is expected for "rare" penguins: $B, B_s \to \phi\gamma, \rho\gamma, \omega\gamma$ and others.

Due to kinematics and a very hard trigger cut on the transverse energy of the photons ($E_T > 4$ GeV), photons under consideration populate a very hard part of the momentum spectrum.

It was shown [5] that it is quite possible to reconstruct about 27k of $B \to K^*\gamma$ events per year with a signal to background ratio close to unity

$\frac{\mathcal{S}}{\mathcal{B}} \sim 1$. Unfortunately uncertainties in this ratio are large, and especially unclear for "rare" penguins. One can expect, for example $\frac{\mathcal{S}}{\mathcal{B}}$ for the decay $B \to \rho\gamma$ to be an order of magnitude worse due to the smaller branching ratio. Additional degradation is expected from the large natural width of the ρ resonance and large combinatorial background for di-pion system. Therefore even $\frac{\mathcal{S}}{\mathcal{B}} \sim 1$ for the decay $B \to K^*\gamma$ is not sufficient for detailed investigations of rare radiative penguins. Looking at the details of the analysis in [5] one concludes that the abilities of the electromagnetic calorimeter are only partially exploited for the $\gamma - \pi^0$ separation. An additional (almost independent of all other details of analysis) factor of background reduction can be obtained using a detailed study of $\gamma - \pi^0$ separation at high energies.

We have chosen this subtask for optimization of the inner section of the electromagnetic calorimeter. We have compared the performance of 4×4 cm and 6×6 cm cells in view of separation between overlapped π^0s and prompt photons. As a separation tool we have chosen the Neural Network approach using the program `JETNET` [6][7]. First we have generated special samples of γs and π^0s in the presence of all other calorimeter activity. The particles were required to satisfy the following criteria (see also table 6 for efficiencies):

- a particle (γ or π^0) should form one local maximum – one cluster
- the collected energy from a matrix 5×5 should exceed the 90% of initial Monte Carlo energy of the initial particle.

Table 6: Percentages of the events satisfying the selection criteria and used in Neural Network analysis

Energy of γ/π^0	$\epsilon^{\gamma}_{4\times4\text{ cm}}$	$\epsilon^{\gamma}_{6\times6\text{ cm}}$	$\epsilon^{\pi^0}_{4\times4\text{ cm}}$	$\epsilon^{\pi^0}_{6\times6\text{ cm}}$
50 GeV	78%	76%	18%	45%
60 GeV	78%	78%	31%	52%
70 GeV	79%	80%	43%	56%
80 GeV	80%	80%	51%	59%
90 GeV	80%	80%	55%	61%
100 GeV	80%	80%	58%	64%

The results of the Neural Network analysis are presented in figure 2 for 50, 60, 70, 80, 90 and 100 GeV particles. The suppression factors for π^0 as a function of prompt photon identification are shown in these figures.

[7]See also appendix B.

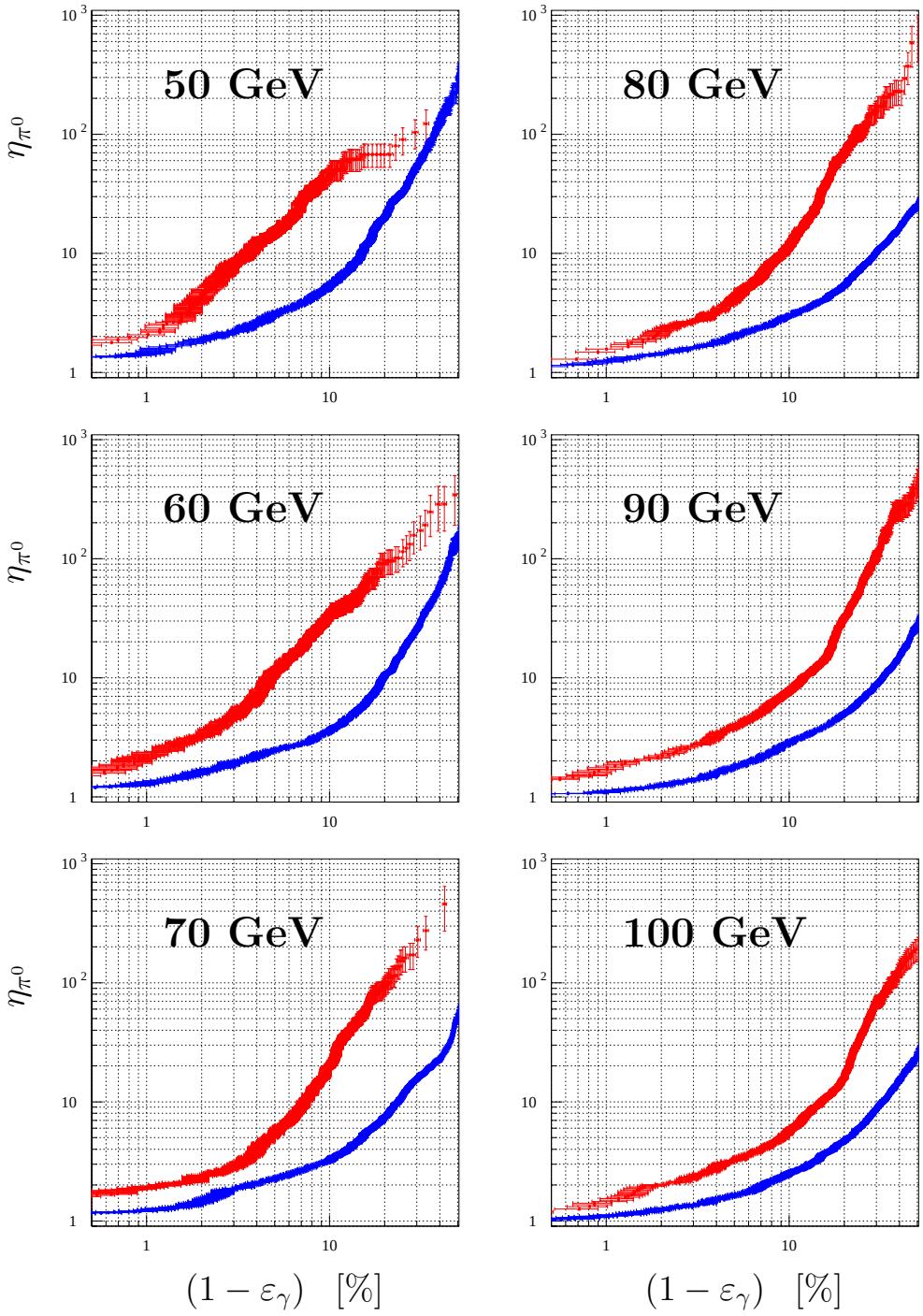

Figure 2: γ/π^0 separation with Neural Network analysis. The dependence of the overlapped π^0s suppression factor on the inefficiency of prompt photons detection is shown. The upper (red) points correspond to 4×4 cm cells, the lower (blue) points correspond to 6×6 cm cells

Suppression factors as function of particle energy are listed in table 7, for the values of prompt photon identification efficiency fixed to 95%,90% and 80%. The 4×4 cm cells demonstrate a significantly better π^0 rejection as compared to 6×6 cm cells (factor 2-10 depending on momentum) confirming our choice of the 4-12 design.

Table 7: Suppression factor for π^0 as a function of particle energy for 95%,90% and 80% photon identification efficiency for different cell sizes in the inner calorimeter

Energy	ε_γ	6×6 cm	4×4 cm
50 GeV	95%	3.0	$\sim$15
60 GeV	95%	2.5	$\sim$10
70 GeV	95%	2.2	$\sim$5.5
80 GeV	95%	2.0	$\sim$4
90 GeV	95%	1.8	$\sim$4
100 GeV	95%	1.6	$\sim$3.2
50 GeV	90%	5.5	$\sim$50
60 GeV	90%	4.5	$\sim$35
70 GeV	90%	3.0	$\sim$20
80 GeV	90%	3.0	$\sim$10
90 GeV	90%	3.0	$\sim$8
100 GeV	90%	2.5	$\sim$6.5
50 GeV	80%	20	$\sim$75
60 GeV	80%	10	$\sim$75
70 GeV	80%	7.0	$\sim$75
80 GeV	80%	5.0	$\sim$70
90 GeV	80%	5.0	$\sim$30
100 GeV	80%	4.5	$\sim$15

7 Conclusions

Optimisation has been done for the granularity of the electromagnetic calorimeter. Performance of representative decay channels ($B \to \rho\pi$, $B \to DK^*$, $b \to \gamma X$) competes with the cost and simplicity considerations. The two section electromagnetic calorimeter with 4x4 (inner zone) and 12x12 cm (outer zone) cells is considered to be the optimal choice. More detailed studies of the innermost region of the outer ECAL section where reconstruction of π^0s suffers from pile-up effect are in progress.

Appendix

A Impact of pile-up and feed-down on π^0 and B^0 reconstruction in $B \to \rho\pi$ decay mode

Table 8 shows definitions of approximations used for $\pi^0 \to \gamma\gamma$ reconstruction.

Table 8: Approximations for $\pi^0 \to \gamma\gamma$ reconstruction

Option	Pile-up	Feed-down
Ideal I	no	no
Ideal II	no	included
Ideal III	included	no
Real I	included	included
Ideal IIa	no	included, redistributed
Real Ia	included	included, redistributed

Results of reconstruction of $B^0 \to \rho^0\pi^0 \to \pi^+\pi^-\pi^0$ decay are summarized in table 9 for TP-rec option of calorimeter and in table 10 for 4-12 and 6-12 options of calorimeter.

Table 9: B^0 and π^0 reconstruction characteristics for $B^0 \to \rho^0\pi^0$ decay in in TP-rec calorimeter. The effective invariant mass resolution of π^0, the effective mass resolution for B^0 and the reconstruction efficiency of B^0s within $\pm 2\sigma$ are listed in the table

Option	Cells [cm^2]	σ_{π^0} [MeV/c^2]	σ_{B^0} [MeV/c^2]	ε_{B^0} [%]
Ideal I	4×4	5	56	25
Ideal II	4×4	7	98	22
Ideal III	4×4	6	62	22
Ideal IIa	4×4	6	59	24
Real I	4×4	8	112	21
Real Ia	4×4	7	63	21
Ideal I	8×8	7	72	26
Ideal II	8×8	10	97	23
Ideal III	8×8	8	78	24
Ideal IIa	8×8	8	76	25
Real I	8×8	12	108	22
Real Ia	8×8	10	83	23
Ideal I	16×16	8	88	24
Ideal II	16×16	13	100	22
Ideal III	16×16	10	94	21
Ideal IIa	16×16	9	90	22
Real I	16×16	15	118	21
Real Ia	16×16	11	95	19

Table 10: B^0 and π^0 reconstruction characteristics for $B^0 \to \rho^0\pi^0$ decay in NEW-4-12 and NEW-6-12 calorimeters. The effective invariant mass resolution of π^0, the effective mass resolution for B^0 and the reconstruction efficiency of B^0s within $\pm 2\sigma$ are listed in the table

Option	Cells [cm^2]	σ_{π^0} [MeV/c^2]	σ_{B^0} [MeV/c^2]	ε_{B^0} [%]
Ideal I	4×4	5	54	25
Ideal II	4×4	8	99	23
Ideal III	4×4	6	59	22
Ideal IIa	4×4	6	58	24
Real I	4×4	9	113	21
Real Ia	4×4	7	64	22
Ideal I	6×6	6	63	14
Ideal II	6×6	12	106	12
Ideal III	6×6	8	71	11
Ideal IIa	6×6	9	63	13
Real I	6×6	14	111	10
Real Ia	6×6	10	72	10
Ideal I	12×12 (I)	8	92	14
Ideal II	12×12 (I)	14	133	13
Ideal III	12×12 (I)	9	113	12
Ideal IIa	12×12 (I)	11	96	14
Real I	12×12 (I)	19	162	13
Real Ia	12×12 (I)	14	117	12
Ideal I	12×12 (II)	8	89	35
Ideal II	12×12 (II)	9	108	32
Ideal III	12×12 (II)	8	93	33
Ideal IIa	12×12 (II)	8	93	33
Real I	12×12 (II)	10	109	30
Real Ia	12×12 (II)	9	95	31

B Neural Network method description

For this analysis we have chosen 6 variables, each variable was normalised to the total energy deposition in the 5×5 matrix. All variables are listed in table 11. Index c (e.g. $E^c_{3\times3}$) implies that this sub-matrix is centred with respect to the initial 5×5 matrix. Index $*$ (e.g. $E^*_{2\times3}$) implies that the choice of corresponding sub-matrix is ambiguous, in that case we choose one with a maximum energy deposition.

Table 11: Input variables (normalised to the total energy deposition in the 5×5 matrix) for Neural Network analysis

Variable	Name	Definition
1	`var1`	$E^c_{1\times1}$
2	`var2`	$\max_4(E^*_{1\times2})$
3	`var3`	$\max_4(E^*_{2\times2})$
4	`var4`	$\max_4(E^*_{2\times3})$
5	`var5`	$E^c_{3\times3}$
6	`var6`	$\max_4(E^*_{4\times4})$

Net architecture includes 3 layers - input layers with 6 input node, hidden layer with 6 nodes and output layer with 1 output node. Net were trained to give 0 on the output node for photons and to produce 1 on the output node for overlapped π^0. In total we have prepared 12 nets - for each fixed initial energy of the particle and for 2 cell sizes 4×4 cm and 6×6 cm. For a training of the net we have used default parameters of the `JETNET` program with back-propagation method. Training samples include 2000 photons (after cuts) and 2000 pions (also after cuts). Possible pile-up was added. The training cycle was 1000 epochs, corresponding to 4000 patterns per epoch. Updating rate was adjusted to be 10 patterns per update, corresponding to 400 updates per epoch.

Statistically independent samples of photons and pions with pile-up for net testing were 1500-5000 patterns depending on energy and cell size.

List of Tables

List of Figures

References

[1] LHCb Technical Proposal, CERN/LHCC 98-4, LHCC/P4, Feb. 1998

[2] I. Korolko, internal presentation, LHCb note in preparation

[3] A. Jacholkowska, internal presentation, LHCb note in preparation

[4] Particle Data Group, The European Physical Journal C3 (1998) 1.

[5] P. Pakhlov and G. Kostina, High Et photon trigger. LHCb TRIG 97-015
P. Pakhlov and G. Kostina, Radiative B decays. LHCb PHYS 97-022

[6] C. Peterson, Th. Rognaldsson and L. Lonnblad, CERN-TH-7135/94, Dec. 1993